ACS Photonics

Letter

pubs.acs.org/journal/apchd5

Enantioselective Optical Trapping of Chiral Nanoparticles with Plasmonic Tweezers

Yang Zhao,*[,†] Amr A. E. Saleh,[†,‡] and Jennifer A. Dionne*[,†]

[†]Materials Science and Engineering and [‡]Electrical Engineering, Stanford University, Stanford, California 94305, United States

Supporting Information

ABSTRACT: Enantiomer separation is a critical step in many chemical syntheses, particularly for pharmaceuticals, but prevailing chemical methods remain inefficient. Here, we introduce an optical technique to sort chiral specimens using coaxial plasmonic apertures. These apertures are composed of a deeply subwavelength silica channel embedded in silver and can stably trap sub-20 nm dielectric nanoparticles. Using both full-field simulations and analytic calculations, we show that selective trapping of enantiomers can be achieved with circularly polarized illumination. Opposite enantiomers experience distinct trapping forces in both sign and magnitude: one is trapped in a deep potential well, while the other is repelled with a potential barrier. These potentials maintain opposite signs across a range of chiral polarizabilities and enantiomer−aperture separations. Our theory indicates that the interaction of chiral light and chiral specimens can be mediated by achiral plasmonic apertures, providing a possible route toward all-optical enantiopure syntheses.

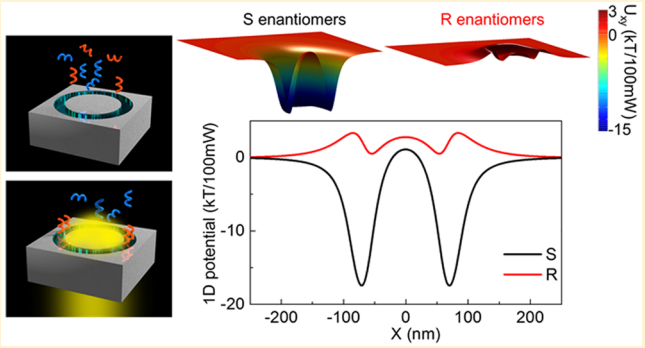

KEYWORDS: *optical forces, nano-optical tweezers, enantiomer separation, chiral molecules*

Molecular chirality is strongly related to biological function. For example, when a chiral molecule such as a protein loses its original chirality, it can become toxic to cells, a process that has been suggested as one of the underlying causes of many diseases including Alzheimer's, Parkinson's, Huntington's, and type II diabetes.[1] Further, because cellular receptors normally target specific molecular chiralities, enantiopure drugs are often more effective and produce considerably fewer side effects than their racemic counterpart.[2] Since enantiomers are identical in their chemical composition and scalar physical properties, existing separation methods such as chiral chromatography rely on the unique ways in which each molecule in an enantiomeric pair interacts with other chiral molecules.[3,4] These chemical processes may introduce unwanted side products and, perhaps more importantly, have a low selectivity and a poor atom economy.

Light can be a less invasive and more efficient alternative to chemical methods for separating enantiomers. It has been shown recently that optical forces[5,6] on an enantiomeric pair of chiral particles are distinct due to the opposite sign in their chiral polarizabilities.[7−13] For example, Tkachenko et al. showed that micrometer-sized chiral particles illuminated with circularly polarized light can feel different forces that drag these particles toward opposite directions depending on their handedness.[10] However, to date, this mechanism can separate only particles that are considerably larger than proteins and pharmaceutically relevant molecules, owing to the weak nature of optical forces exerted on nanometer-sized specimens. These optical forces can be increased using plasmonic optical tweezers, which rely on enhanced near-field gradients. Using plasmonic tweezers, direct optical manipulation of sub-100 nm particles and proteins[14−22] has been achieved, but these traps are indiscriminate to particle chirality. Here we show how enantioselective optical trapping can be achieved at the nanoscale by combining chiral optical forces with efficient plasmonic tweezers. We design an achiral plasmonic coaxial nanoaperture to selectively trap sub-10 nm dielectric specimens based on their chirality. Our calculations show that this scheme achieves significant differences in trapping potentials that stably trap one enantiomer of the pair while repelling the other.

In general, optical forces on a particle can be written as[23−25]

$$\mathbf{F} = \mathrm{Re}\{(\mathbf{p}\cdot\nabla)\mathbf{E} + (\mathbf{m}\cdot\nabla)H + \mu_0\dot{p} \times \mathbf{H} - \varepsilon_0\dot{m} \times \mathbf{E}\} \quad (1)$$

where $\mathbf{p}$ and $\mathbf{m}$ are the electric and magnetic dipole moments, $\mathbf{E}$ and $\mathbf{H}$ are the electric and magnetic fields, and μ_0 and ε_0 are the permeability and permittivity of vacuum. The electric and magnetic dipole moments are related to the incident fields by the polarizability tensor of the particle as given in eq S1 in the Supporting Information. A chiral particle can be modeled as a pair of interacting electric and magnetic dipoles. This interaction is manifest in its electromagnetic polarizability α_{em}, which is closely related to the chirality (κ) of the particle as

Received: October 6, 2015
Published: February 23, 2016

DOI: 10.1021/acsphotonics.5b00574
ACS Photonics 2016, 3, 304−309

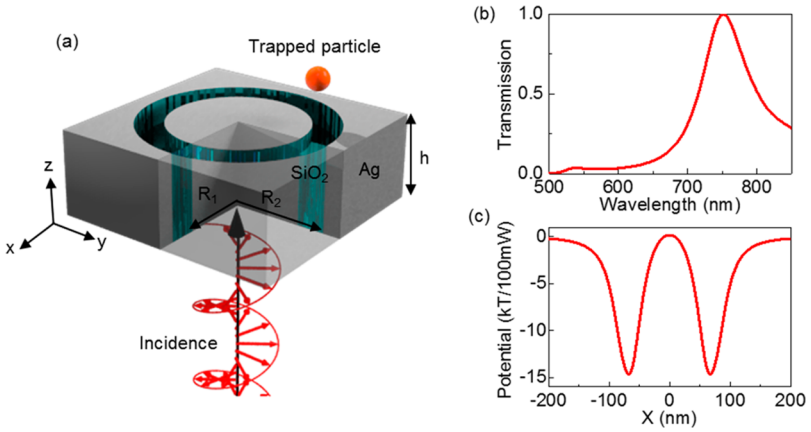

Figure 1. (a) Schematic view of the plasmonic coaxial aperture, with R_1 = 60 nm, R_2 = 85 nm, h = 150 nm. The incident light is left-handed circularly polarized and propagates along the +z direction. (b) Finite difference time domain simulation (FDTD, Lumerical) of the normalized transmission coefficient for the coaxial aperture. (c) One-dimensional trapping potential on an achiral particle with a refractive index of 1.45 and a diameter of 20 nm in water, 20 nm above the aperture. The trapping potential is normalized to 100 mW transmitted power.

$\alpha_{em} = -12\pi r^3 \frac{j\kappa\sqrt{\mu_0\varepsilon_0}}{(\varepsilon_r + 2\varepsilon_{rm})(\mu_r + 2\mu) - \kappa^2}$, where r is the particle radius, ε_r (μ_r) is the relative permittivity (permeability) of the particle, and ε_{rm} is the relative permittivity of the medium (Supporting Information).[26] The chirality κ is a dimensionless parameter that measures the degree of the handedness of chiral materials.[26]

As eq 1 indicates, optical forces relate not only to the electric and magnetic field gradients but also to the spin- and orbital-angular momentum of the fields.[24] For chiral specimens, the latter contribution is different for different enantiomers. Consequently, we use this term to separate enantiomers with different chiralities. To illustrate this effect, we first focus on the transverse optical forces (the forces generated in the x−y plane as illustrated in Figure 1). They can be simplified in terms of the polarizability of the particles as[11]

$$\mathbf{F}_{tr} = \frac{\mathrm{Re}(\alpha_{ee})}{4}\nabla|\mathbf{E}|^2 + \mathrm{Im}(\alpha_{ee})\left(\frac{\omega}{2\varepsilon_0}\nabla \times \mathbf{L}_s\right) + \mathrm{Im}(\alpha_{em})\frac{1}{2}\nabla\mathrm{Im}(\mathbf{E}\cdot\mathbf{H}^*) - \mathrm{Re}(\alpha_{em})\nabla \times \mathbf{S} \quad (2)$$

where α_{ee} is the electric polarizability, $\mathbf{L}_s$ is the spin angular momentum, and $\mathbf{S}$ is the Poynting vector. In eq 2, the force terms can be classified as follows: the first term is the gradient force; the second term is the curl-spin force;[11,27] the third term is the chiral gradient force; and the fourth term is the vortex force.[11] It is important to note that these four force components may not contribute simultaneously or equally. This equation can be further simplified for the case of a small chiral particle within the quasi-static limit under two conditions. First, to trap biological targets, the trapping laser needs to be in the visible to near-IR region, which coincides with the first optical window to avoid their heating damage. For small specimens (i.e., diameters in the range of a few nanometers), their Mie resonances are commonly located in the UV region, far from the trapping wavelength. Under this condition, the curl-spin force that is related to $\mathrm{Im}(\alpha_{ee})$ becomes negligible.[25,27] Second, the circular dichroism (CD) of the specimen, which is related to $\mathrm{Re}(\alpha_{em})$, normally peaks in the UV region for small chiral particles. In contrast, the optical rotational dispersion (ORD) is related to $\mathrm{Im}(\alpha_{em})$ and extends to much longer wavelengths.[28,29] Therefore, the vortex force also vanishes when the trapping wavelength is far from the UV. With these considerations, the transverse optical force on chiral nanoparticles reduces to

$$\mathbf{F}_{tr} \approx \frac{\mathrm{Re}(\alpha_{ee})}{4}\nabla|\mathbf{E}|^2 + \mathrm{Im}(\alpha_{em})\frac{1}{2}\nabla\mathrm{Im}(\mathbf{E}\cdot\mathbf{H}^*) \quad (3)$$

Note that the gradient chiral force (the second term in eq 3) changes sign when enantiomers are trapped because of their opposite signs in ORD. As a result, the difference between the trapping forces of an enantiomeric pair comes from the *addition* or *subtraction* between the two force components in eq 3. In the following, we will refer to the first part of the transverse force as the *dielectric* gradient force and the second part as the *chiral* gradient force since it is directly related to the optical chirality density ($\mathrm{Im}(\mathbf{E}\cdot\mathbf{H}^*)$) of the field.[30,31] Equation 3 indicates that apertures that provide a large gradient of the optical chirality density can result in strong contrasts in their optical forces on chiral objects with opposite handedness.

We chose a coaxial nanoaperture as our design, because it is a plasmonic resonant structure[32−34] that provides large field gradients in the transverse plane. Recently, we have theoretically demonstrated that field gradients near this coaxial aperture are large enough to generate piconewton forces for dielectric particles as small as 2 nm.[22] This force leads to a trapping potential depth larger than 10 kT, which is enough to oppose the Brownian motion of the nanoparticles suspended in solution. Since the two components of the transverse forces for chiral objects in eq 3 are essentially based on field gradients, this coaxial structure shows great promise to trap a small chiral object. Most importantly, we will show that the circular symmetry of the aperture is crucial to the *addition* or *subtraction* between the two force components in eq 3 for separating enantiomers.

The coaxial nanoaperture we consider has a silver[35] core of radius R_1 = 60 nm, a silicon dioxide ring that extends to a radius R_2 = 85 nm, and a thickness h = 150 nm, as schematically shown in Figure 1a. Upon illumination with circularly polarized light, the transmission spectrum of this structure peaks at two wavelengths corresponding to the Fabry−Perot resonances of this structure shown in Figure 1b. In this study, we use the stronger resonance at λ = 751 nm, which is the fundamental plasmon mode when the specimen is in water (n = 1.33). Figure 1c shows the one-dimensional trapping potential on an *achiral* nanoparticle using this aperture with left-handed

DOI: 10.1021/acsphotonics.5b00574
ACS Photonics 2016, 3, 304−309

circularly polarized illumination. With a refractive index of 1.45 and a diameter of 20 nm, the trapping potential depth for this particle is −14.7 kT with 100 mW transmitted power in water.

To analyze whether this structure can provide an enantioselective optical force, we employ a semianalytical approach by first investigating the field distributions close to the aperture surface using finite difference time domain (FDTD) simulations. Then we introduce a chiral particle, whose polarizabilitites are estimated based on the quasi-static limit, and calculate the total transverse forces experienced by this particle based on eq 3. This approach assumes that the chiral specimens do not perturb the fields, which is typical for specimens that are much smaller than the aperture and within the Rayleigh regime ($r_{\text{specimen}} \ll \lambda/20$). In the following we model our targeted chiral specimen as a spherical nanoparticle with a diameter of 20 nm, a dielectric constant of 1.45, and a chirality (κ) in the range between −1.45 and +1.45 with the plus (minus) sign indicating S (R) enantiomers, corresponding to an electromagnetic polarizability α_{em} in the range of $\left(-\frac{3.69}{c} \times 10^{-24}\ \text{m}^3, +\frac{3.69}{c} \times 10^{-24}\ \text{m}^3\right)$, with c being the speed of light in vacuum. Such polarizabilities span the range of common chiral specimens including DNA-assembled nanostructures and composite nanomaterials with similar dimensions.[8,36−42]

To analyze the field profile and subsequent forces from the coaxial nanoaperture, we first illuminate the aperture with linearly polarized light along the y direction. In Figure 2, we show one example of the transverse forces on an enantiomeric pair with a chirality κ of ±0.6, corresponding to an electromagnetic polarizability of $\sim \frac{1.37}{c} \times 10^{-24}\ \text{m}^3$. Figure 2a shows the magnitude of the dielectric gradient force on an S enantiomer in the x−y plane, overlaid with a quiver plot showing the directions of this force. This force map is obtained through FDTD simulations by placing the monitor 20 nm above the coaxial aperture. In Figure 2a, the gray arrows indicate this dielectric gradient force (arising from the electrical field gradient ($\nabla|\boldsymbol{E}|^2$) is concentrated along the direction of the input polarization, allowing trapping of the specimen explicitly above the dielectric channel of the coaxial structure. Figure 2b shows the spatial variation of the chiral gradient force on the same S enantiomer. Note the hot spots overlap with the maxima of the chirality density gradient ($\nabla\text{Im}(\mathbf{E}\cdot\mathbf{H}^*)$), which are located at different points on the ring from the maxima of the electrical field gradient. This spatial separation jeopardizes the possibility of annihilating the total transverse force for one enantiomer while enhancing the forces for the other one to achieve force-induced separation. As a result, the transverse forces through the nanoaperture with linearly polarized excitation will have the same magnitude for both the S and R enantiomers, shown in Figure 2c and d.

To solve this problem caused by the unmatched maxima from the electrical field gradient and the chirality density gradient as indicated by Figure 2a and b, it is necessary to match the symmetry between the nanoaperture and the field distribution. Therefore, instead of linearly polarized light, a circularly polarized source is used in our scheme. In Figure 3a and b, we show these force components on the S enantiomers again, but with left-handed circularly polarized (LCP) excitation

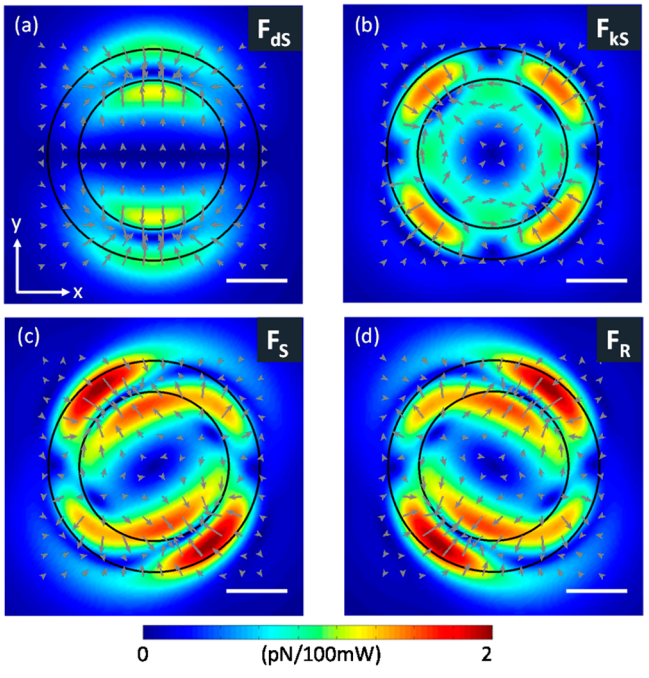

Figure 2. Calculated transverse forces 20 nm above the aperture with linearly polarized illumination. The dielectric channel of the aperture is outlined by the concentric black circles. The color map shows force magnitude, and the gray arrows show force directions. (a) Dielectric gradient force for the S enantiomers (denoted as F_{dS}). (b) Chiral gradient force for the S enantiomers (denoted as F_{kS}). (c) Total transverse force for the S enantiomers (F_S). (d) Total transverse force for the R enantiomers (F_R). The particle chirality is $\kappa = \pm 0.6$. The scale bars are 50 nm in all panels.

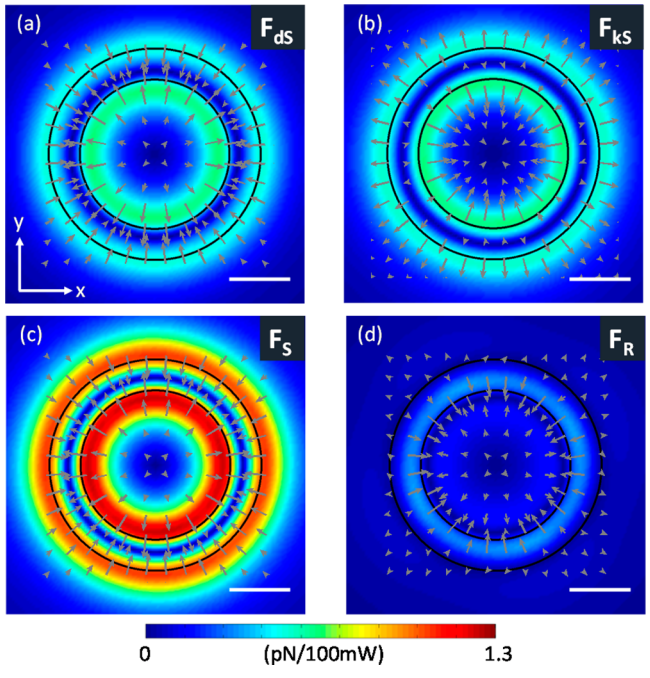

Figure 3. Calculated transverse forces 20 nm above the aperture with left-handed circularly polarized illumination. The dielectric channel of the aperture is outlined by the concentric black circles, the color map shows force magnitude, and the gray arrows show force directions. (a) Dielectric gradient force for the S enantiomers (denoted as F_{dS}). (b) Chiral gradient force for the S enantiomers (denoted as F_{kS}). (c) Total transverse force for the S enantiomers (F_S). (d) Total transverse force for the R enantiomers (F_R). The particle chirality is $\kappa = \pm 0.6$ for this figure. The scale bars are 50 nm in all panels.

DOI: 10.1021/acsphotonics.5b00574
ACS Photonics 2016, 3, 304−309

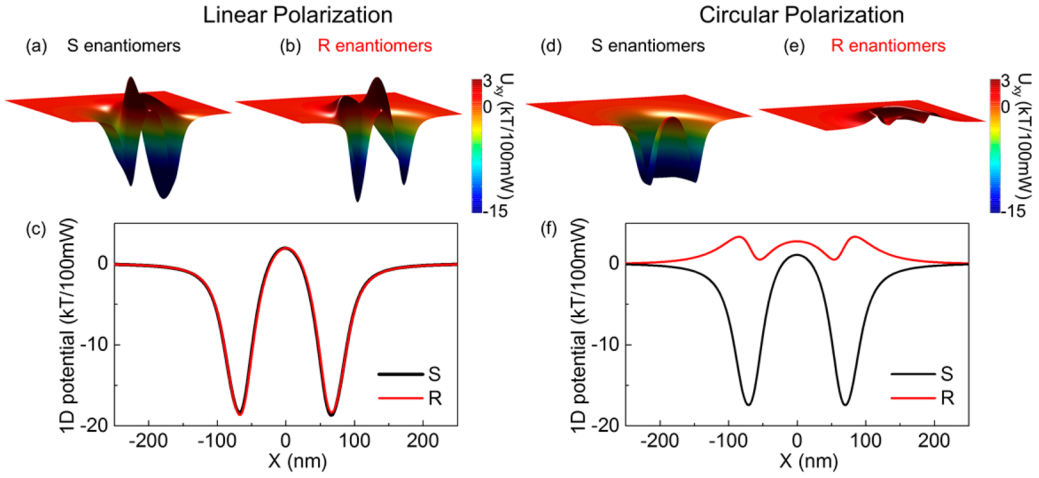

Figure 4. Trapping potentials for enantiomers with linear and circular polarizations. Two-dimensional (2D) trapping potential with linearly polarized incidence for (a) *S* enantiomers and (b) *R* enantiomers at 20 nm above the nanoaperture. (c) One-dimensional (1D) trapping potentials across the aperture at 20 nm above the aperture for both *R* and *S* enantiomers. (d, e, and f) Corresponding 2D and 1D trapping potentials with left-handed circularly polarized illumination. The particle chirality is $\kappa = \pm 0.6$ for this figure. For the cases with circularly polarized illumination, distinctions of potentials between the *S* (black curves) and *R* (red curves) enantiomers provide selectivity to trap only one enantiomer (the *S* enantiomers as shown here).

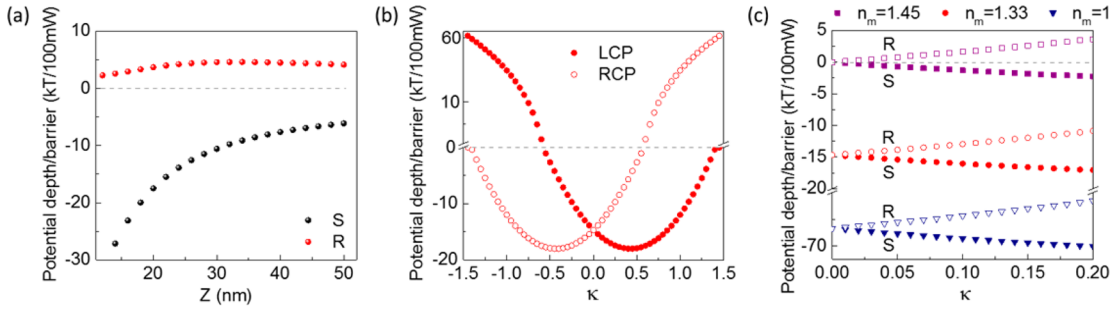

Figure 5. (a) Depth of trapping potentials for *S* and *R* enantiomers with chirality $\kappa = \pm 0.6$ as a function of distance away from the aperture. (b) Trapping potential depth and barrier as a function of chirality at $z = 20$ nm above the aperture with left-handed (solid symbols) and right-handed (open symbols) circularly polarized incidence. For clarity, the *y* axis breaks between 0 and 3 kT. Below the break, the *y* axis is in linear scale; after the break, the *y* axis is in log scale. (c) Potential depth and barrier as a function of chirality and refractive index of the medium (n_m) in which the nanoparticle is immersed. The illumination is left-handed circularly polarized light. *R* (and all open symbols) denotes *R* enantiomers, and *S* (solid symbols) denotes *S* enantiomers. The *y* axis breaks between −60 and −20 kT for clarity. In all panels, the gray dashed line indicates 0 kT potential.

to the aperture. With LCP excitation, the maxima for both the electric field gradient and the chiral density gradient now coincide at the ring channel of the aperture. With the same chiral particles with $\kappa = \pm 0.6$, it is seen that for the *S* enantiomers the total maximum transverse force now reaches 1.23 pN/100 mW, attracting the particle toward the dielectric channel. For the *R* enantiomers, the force is only 0.35 pN/100 mW in magnitude. Moreover, as indicated by the gray arrows, the transverse forces push the particle toward the coaxial channel for the *S* enantiomer, enabling trapping, but away from the channel for the *R* enantiomer.

The drastic differences in the magnitude and sign of the optical forces for the enantiomeric pair result in a large difference in their trapping potentials. Figure 4 depicts the trapping potentials of the enantiomers with both linearly (panels a–c) and circularly polarized light (panels d–f). Figure 4a shows the three-dimensional perspective view of the calculated two-dimensional (2D) trapping potentials on the *S* enantiomers at 20 nm away from the aperture, cut through the x–z plane to reveal the shape of the potential wells. Figure 4b shows the same trapping potentials on the *R* enantiomers, again cut through in the x–z plane. Figure 4c shows the one-dimensional (1D) trapping potentials along the x directions across the aperture for both enantiomers. With linearly polarized illumination, the aperture provides exactly the same trapping potentials for both enantiomers. On the contrary, with a circularly polarized illumination (e.g., LCP illumination here), the same aperture provides a trapping potential as deep as −17 kT at 20 nm above the aperture for the *S* enantiomers, while for the *R* enantiomers the trapping potential is positive at the same location. This distinct trapping potential stably captures only the *S* enantiomers near the aperture, such that the untrapped *R* enantiomers can be washed away to produce a purely *S* enantiomer solution. To trap the other handedness, one may simply reverse the incidence polarization to right-handed circularly polarized light. Then the same forces and trapping potentials for the *S* enantiomers would apply to the *R* enantiomers.

Since this trapping is a near-field effect, the trapping potential decays when the particles are positioned farther away from the aperture. Figure 5a shows the maximum trapping potential depth or barrier as a function of the distance away from the aperture for a pair of enantiomers with $\kappa = \pm 0.6$. Although the trapping potential depth decreases for the *S* enantiomers as the

DOI: 10.1021/acsphotonics.5b00574
ACS Photonics 2016, 3, 304–309

particle−aperture separation increases, the potential barriers for the *R* enantiomers remain positive. Therefore, only the *S* enantiomers will be trapped when the aperture is illuminated with LCP light, regardless of specimen distance above the aperture. Stable trapping occurs when the particles are within 20 nm of the aperture.

In the above analysis, we have chosen a fixed chirality of the particle. In Figure 5b, we show the maxima of the trapping potential depth as a function of chirality κ with both left-hand (LCP) and right-hand incident polarizations (RCP) at z = 20 nm away from the aperture. Figure 5 indicates the current geometry of the nanoaperture can provide stable trapping of *S* enantiomers with LCP incident light for chiral specimens with chirality between 0.2 and 1. However, this chirality is still much larger than that of a natural chiral material. To extend the current trapping scheme, the nanoparticle can be immersed in a medium with a matched refractive index. Such index-matching improves the enantioselectivity because it reduces the contribution of the *dielectric* gradient forces while maintaining the differences between the *chiral* gradient forces. Notably, when the same chiral particle is immersed in a higher refractive index medium, the ratio between polarizabilities $(\frac{\mathrm{Re}(\alpha_{ee})}{\mathrm{Im}(\alpha_{em})})$ is lowered (see Figure S2 in the Supporting Information). As shown in Figure 5c, a reduced index contrast between the particle and the surrounding medium reduces the depth of the potential well, but maintains the difference between the trapping potentials of the enantiomers. When the index of the medium matches that of the particle, the contribution of the *dielectric* gradient force in eq 3 is minimized; consequently, the coaxial aperture traps only one enantiomer while repelling the other for any nonzero chirality.

In conclusion, we have shown that selective optical trapping of small particles based on their chiralities is theoretically possible using a properly designed nanoaperture. Our results show that our current aperture design can stably trap *S* enantiomers with matched handedness of the incident light within 20 nm from the aperture, while the *R* enantiomers remain untrapped due to a positive trapping potential at the same locations. This feature precludes the necessities to consider the pulling forces in the z direction, although our calculations show that the pulling forces are enhanced for the *S* enantiomers and reduced for the *R* enantiomers (see Figure S1 in the Supporting Information). Our design provides an alternate route toward enantiopure chemical syntheses and enantiomer separations in pharmaceuticals. The potential impact of this technique extends beyond pharmaceutical development to a single-particle sensor that can detect and trap chiral specimens with a specific chirality at low concentrations. Using such probes, one can trace chirality changes of a single chiral particle or molecule and study its dynamic interactions with other chiral compounds.

■ ASSOCIATED CONTENT

Supporting Information

The Supporting Information is available free of charge on the ACS Publications website at DOI: 10.1021/acsphotonics.5b00574.

Analysis of chirality κ, longitudinal forces, and polarizabilities as a function of the immersed medium (PDF)

■ AUTHOR INFORMATION

Corresponding Authors

*E-mail: yangzhao@stanford.edu.
*E-mail: jdionne@stanford.edu.

Notes

The authors declare no competing financial interest.

■ ACKNOWLEDGMENTS

The authors acknowledge the Gordon and Betty Moore Foundation for funding support, and Aitzol Garcia and Hadiseh Alaeian for useful discussions.

■ REFERENCES

(1) Dobson, C. M. Protein folding and misfolding. *Nature* **2003**, *426*, 884−890.
(2) Smith, S. W. Chiral toxicology: it's the same thing···only different. *Toxicol. Sci.* **2009**, *110*, 4−30.
(3) Ward, T. J.; Baker, B. A. Chiral separations. *Anal. Chem.* **2008**, *80*, 4363−4372.
(4) Li, B.; Taynie, D. T. In *Encyclopedia of Chemical Processing*, Vol. *1*; Lee, S., Ed.; Taylor & Francis: New York, 2005; pp 449−458.
(5) Ashkin, A. Optical trapping and manipulation of neutral particles using lasers. *Proc. Natl. Acad. Sci. U. S. A.* **1997**, *94*, 4853−4860.
(6) Soltani, M.; Lin, J.; Forties, R. A.; Inman, J. T.; Saraf, S. N.; Fulbright, R. M.; Lipson, M.; Wang, M. D. Nanophotonic trapping for precise manipulation of biomolecular arrays. *Nat. Nanotechnol.* **2014**, *9*, 448−452.
(7) Hayat, A.; Balthasar Müller, J. P.; Capasso, F. Lateral chirality-sorting optical forces. *Proc. Natl. Acad. Sci. U. S. A.* **2015**, *112*, 13190−13194.
(8) Canaguier-Durand, A.; Hutchison, J. A.; Genet, C.; Ebbesen, T. W. Chiral discrimination in optical trapping and manipulation. *New J. Phys.* **2013**, *15*, 123037.
(9) Cameron, R. P.; Barnett, S. M.; Yao, A. M. Discriminatory optical force for chiral molecules. *New J. Phys.* **2014**, *16*, 013020.
(10) Tkachenko, G.; Brasselet, E. Optofluidic sorting of material chirality by chiral light. *Nat. Commun.* **2014**, *5*, 4577.
(11) Wang, S. B.; Chan, C. T. Lateral optical force on chiral particles near a surface. *Nat. Commun.* **2014**, *5*, 4307.
(12) Bradshaw, D. S.; Andrews, D. L. Laser optical separation of chiral molecules. *Opt. Lett.* **2015**, *40*, 677−680.
(13) Bradshaw, D. S.; Andrews, D. L. Electromagnetic trapping of chiral molecules: orientational effects of the irradiating beam. *J. Opt. Soc. Am. B* **2015**, *32*, 25−31.
(14) Berthelot, J.; Acimovic, S. S.; Juan, M. L.; Kreuzer, M. P.; Renger, J.; Quidant, R. Three-dimensional manipulation with scanning near-field optical nanotweezers. *Nat. Nanotechnol.* **2014**, *9*, 295−299.
(15) Kotnala, A.; Gordon, R. Double nanohole optical tweezers visualize protein p53 suppressing unzipping of single DNA-hairpins. *Nano Lett.* **2014**, *14*, 853−856.
(16) Pang, Y.; Gordon, R. Optical trapping of a single protein. *Nano Lett.* **2012**, *12*, 402−406.
(17) Zheng, Y.; Ryan, J.; Hansen, P.; Cheng, Y.; Lu, T.; Hesselink, L. Nano-optical conveyor belt, part II: demonstration of handoff. *Nano Lett.* **2014**, *14*, 2971−2976.
(18) Wang, K.; Schonbrun, E.; Steinvurzel, P.; Crozier, K. B. Trapping and rotating nanoparticles using a plasmonic nano-tweezer with an integrated heat sink. *Nat. Commun.* **2011**, *2*, 1480.
(19) Wheaton, S.; Gordon, R. Molecular weight characterization of single globular proteins using optical nanotweezers. *Analyst* **2015**, *140*, 4799−4803.
(20) Roxworthy, B.; Ko, K.; Kumar, A.; Fung, K.; Chow, E.; Liu, G.; Fang, N.; Toussaint, K. Application of plasmonic bowtie nanoantenna arrays for optical trapping, stacking, and sorting. *Nano Lett.* **2012**, *12*, 796−801.
(21) Juan, M. L.; Righini, M.; Quidant, R. Plasmon nano-optical tweezers. *Nat. Photonics* **2011**, *5*, 349−356.

DOI: 10.1021/acsphotonics.5b00574
ACS Photonics 2016, 3, 304−309

(22) Saleh, A. A. E.; Dionne, J. A. Toward efficient optical trapping of sub-10-nm particles with coaxial plasmonic apertures. *Nano Lett.* **2012**, *12*, 5581−5586.
(23) Guzatov, D. V.; Klimov, V. V. The influence of chiral spherical particles on the radiation of optically active molecules. *New J. Phys.* **2012**, *14*, 123009.
(24) Bekshaev, A. Y. Subwavelength particles in an inhomogeneous light field: optical forces associated with the spin and orbital energy flows. *J. Opt.* **2013**, *15*, 044004.
(25) Liberal, I.; Ederra, I.; Gonzalo, R.; Ziolkowski, R. W. Electromagnetic force density in electrically and magnetically polarizable media. *Phys. Rev. A: At., Mol., Opt. Phys.* **2013**, *88*, 053808.
(26) Lindell, I. V.; Sihvola, A. H.; Tretyakov, S. A.; Viitanen, A. J. *Electromagnetic Waves in Chiral and Bi-isotropic Media*, 1st ed.; Artech House: London, 1994.
(27) Liberal, I.; Ederra, I.; Gonzalo, R.; Ziolkowski, R. W. Near-field electromagnetic trapping through curl-spin forces. *Phys. Rev. A: At., Mol., Opt. Phys.* **2013**, *87*, 063807.
(28) Adler, A. J.; Greenfield, N. J.; Fasman, G. D. Circular dichroism and optical rotatory dispersion of proteins and polypeptides. *Methods Enzymol.* **1973**, *27*, 675−735.
(29) Moscowitz, A. In *Optical Rotatory Dispersion*; Djerassi, C., Ed.; McGraw-Hill: New York, 1960; p 150.
(30) Tang, Y. Q.; Cohen, A. E. Optical chirality and its interaction with matter. *Phys. Rev. Lett.* **2010**, *104*, 163901.
(31) Garcia-Etxarri, A.; Dionne, J. Surface-enhanced circular dichroism spectroscopy mediated by nonchiral nanoantennas. *Phys. Rev. B: Condens. Matter Mater. Phys.* **2013**, *87*, 235409.
(32) Khajavikhan, M.; Simic, A.; Katz, M.; Lee, J. H.; Slutsky, B.; Mizrahi, A.; Lomakin, V.; Fainman, Y. Thresholdless nanoscale coaxial lasers. *Nature* **2012**, *482*, 204−207.
(33) van de Haar, M. A.; Maas, R.; Schokker, H.; Polman, A. Experimental realization of a polarization-independent ultraviolet/visible coaxial plasmonic metamaterial. *Nano Lett.* **2014**, *14*, 6356−6360.
(34) Saleh, A.; Dionne, J. Waveguides with a silver lining: Low threshold gain and giant modal gain in active cylindrical and coaxial plasmonic devices. *Phys. Rev. B: Condens. Matter Mater. Phys.* **2012**, *85*, 045407.
(35) Johnson, P. B.; Christy, R. W. Optical constants of the noble metals. *Phys. Rev. B* **1972**, *6*, 4370−4379.
(36) Jaggard, D. L.; Mickelson, A. R.; Papas, C. H. On electromagnetic waves in chiral media. *Appl. Phys.* **1979**, *18*, 211−216.
(37) Shen, X.; Asenjo-Garcia, A.; Liu, Q.; Jiang, Q.; García de Abajo, J.; Liu, N.; Ding, B. Three-dimensional plasmonic chiral tetramers assembled by dna origami. *Nano Lett.* **2013**, *13*, 2128.
(38) Kuzyk, A.; Schreiber, R.; Fan, Z.; Pardatscher, G.; Roller, E.; Högele, A.; Simmel, F.; Govorov, A.; Liedl, T. DNA-based self-assembly of chiral plasmonic nanostructures with tailored optical response. *Nature* **2012**, *483*, 311−314.
(39) Johannessen, C.; Blanch, E. W.; Villani, C.; Abbate, S.; Longhi, G.; Agarwal, N. R.; Tommasini, M.; Lightner, D. A. Raman and ROA spectra of (−)- and (+)-2-Br-Hexahelicene: experimental and DFT studies of a π-conjugated chiral system. *J. Phys. Chem. B* **2013**, *117*, 2221−2230.
(40) Zhao, R.; Koschny, T.; Soukoulis, C. M. Chiral metamaterials: retrieval of the effective parameters with and without substrate. *Opt. Express* **2010**, *18*, 14553.
(41) Pendry, J. B. A chiral route to negative refraction. *Science* **2004**, *306*, 1353.
(42) Barron, L. D. *Molecular Light Scattering and Optical Activity*; Cambridge University Press: New York, 2004.

DOI: 10.1021/acsphotonics.5b00574
ACS Photonics 2016, 3, 304−309